Cell Biol Toxicol (2025) 41:81
https://doi.org/10.1007/s10565-025-10034-6

RESEARCH

Panoramic lead-immune system interactome reveals diversified mechanisms of immunotoxicity upon chronic lead exposure

Yifan Hong · Tianbao Ye · Hui Jiang · Aiting Wang · Boqian Wang · Yiyang Li · Haiyang Xie · Hongyu Meng · Chengxing Shen · Xianting Ding

Received: 19 February 2025 / Accepted: 24 April 2025

Abstract Lead exposure is of high prevalence, and over a billion people are chronically exposed to alarming level of lead. Human immune system is highly vulnerable to lead, but the underlying mechanism remains unknown. Using single-cell mass cytometry and mass spectrometry-based proteomics, we performed a panoramic survey of lead targets at both cellular and molecular levels in murine immune system upon chronic lead exposure. We produced a single-cell landscape of lead, thiol metabolism and lead-induced toxicity across all immune cell types. We found that immune cells with extreme thiol metabolism are the most sensitive upon chronic lead exposure. It shows that CD4 + T cells and neutrophils are the most sensitive to lead, which is due respectively to a molecular mechanism rooted in their characteristic thiol metabolic capacity. Meanwhile, we found that lead accumulation by RBC further inflicted secondary toxicity to RBC phagocytes in spleen, e.g. macrophages and neutrophils. Unlike CD4 + T cells, which can be rescued by supplementation with thiol chelator, lead toxicity in these phagocytes cannot be effectively mitigated by thiol chelators. Overall, it forms a multiscale panoramic lead-immune system interactome upon chronic lead exposure, which provides valuable information for proactive prevention, therapy formulation and public health evaluation.

Keywords Chronic lead exposure · Immunotoxicity · Thiol metabolism · CD4 + T cell · Neutrophil

Yifan Hong, Tianbao Ye and Hui Jiang contributed equally to this work.

Supplementary Information The online version contains supplementary material available at https://doi.org/10.1007/s10565-025-10034-6.

Y. Hong (✉)
School of Life and Health Sciences, Fuyao University of Science and Technology, Fuzhou 350109, People's Republic of China
e-mail: hongyifan@fyust.edu.cn

Y. Hong · T. Ye · H. Jiang · A. Wang · B. Wang · Y. Li · H. Xie · H. Meng · X. Ding (✉)
State Key Laboratory of Oncogenes and Related Genes, Institute for Personalized Medicine, School of Biomedical Engineering, Shanghai Jiao Tong University, Shanghai 200030, People's Republic of China
e-mail: dingxianting@sjtu.edu.cn

T. Ye · C. Shen (✉)
Department of Cardiology, Shanghai Jiao Tong University Affiliated Sixth People's Hospital, Shanghai 200233, People's Republic of China
e-mail: shencx@sjtu.edu.cn

Introduction

Lead (Pb) was introduced thousands of years ago as a byproduct of silver mining, and widely used ever since in various purposes (Smith et al. 2018; Gibbons 2020). The most environmentally influential event

Published online: 07 May 2025

of lead pollution is the addition of tetraethyl lead to gasoline as an antiknock agent, which made a pollution of global scale. Even though leaded gasoline is banned since 1996, environmental residual and many other sources of lead pollution remains (Resongles et al. 2021; Makoni 2021; Sonne et al. 2022; Bellinger 2016). Current baseline blood lead levels in human populations range from 10 to 100 ppb, vary according to country or region (Skerfving and Bergdahl 2015). According to WHO report in 2021, lead causes 1 million death each year, which takes up about half of global chemical caused death (Cisse 2023), and around 1/3 of children globally, which is 815 million, have blood lead level higher than the alert level of 5 μg/dl (50 ppb) (Rees and Richard 2020).

Lead is notorious for its toxic effects on cognitive development and hematopoiesis in children, as well as its toxicity to the immune system (McFarland et al. 2022; Gibson et al. 2022; Marshall et al. 2020). Immune cells are constantly exposed to blood lead, and diverse lead-induced toxicities in various immune cell types have been reported (Fenga et al. 2017). Unfortunately, our understanding of lead-induced immunotoxicities remains mostly at the stage of symptom descriptions. It could be due to the cell type heterogeneity of immune system, and symptoms of immunotoxicity are not as easily perceivable as neural or hematopoietic toxicity. It is widely accepted that there is no safe threshold for lead exposure. Lead can induce immunotoxicity at low concentrations, suggesting biological targets of high specificity. Considering the high prevalence of chronic mild lead exposure in humans, the health hazards of lead on the immune system could have been greatly underestimated. Thus, it is important to clarify the underlying mechanisms behind lead-induced immunotoxicity.

In vitro studies indicate that biological thiols, protein metal-binding sites and nucleic acids are biological targets of lead. Glutathione (GSH) and metallothionein (MT) are major metal scavenging thiols in human. GSH is a highly abundant tripeptide with medium binding affinity to metal, whose metal conjugates can be removed by multidrug resistance protein (MRP) (Leslie 2012; Mielniczki-Pereira et al. 2008). GSH removal of heavy metal can be described by a math model named sequestration-aided passive transport (SAPT) (Hong et al. 2015; Lim et al. 2020). MT is a cysteine-rich protein with extremely high binding affinity to lead (Banci et al. 2010). And about 90% of blood lead locates within red blood cells (RBC), which binds the cysteine-rich zinc-binding site of δ-aminolevulinic acid dehydratase (ALAD) (Mani et al. 2018). Due to atomic similarity, Pb^{2+} also shows high binding affinity to protein Ca^{2+} binding sites, especially those with low coordination number (Kasten-Jolly and Lawrence 2018; Dudev et al. 2018). Furthermore, Pb^{2+} can catalyze phosphodiester cleavage in RNA (Palou-Mir et al. 2017).It removes proton from the 2'-OH of RNA ribose and facilitates breakage of RNA phosphodiester backbone (Pan and Uhlenbeck 1992). Pb^{2+} binding to certain sequences of RNA/DNA forms ribozymes or deoxyribozymes, which can efficiently cut RNA/DNA (Barciszewska et al. 2003; Kim et al. 2007).

Despite all the in vitro studies, less is known about the in vivo interaction between lead and its apt molecular targets in immune cells. The landscape of metal scavenging thiols in immune cells is also unclear. Fortunately, we found that current technology and bioinformation are sufficient to support a systematic proteome-wide survey of lead-immune system interaction, which could help us fill the gap between biochemistry and immunotoxicity of lead.

In this study, we first used mass cytometry (CyTOF) to study the single-cell landscapes of lead accumulation, thiol metabolism and lead's impacts on immune cells. The findings showed that neutrophils, naïve CD4 +T cells and splenic RBC phagocytes are the most susceptible upon lead exposure. Using liquid chromatography mass spectrometry (LC–MS), we examined lead-induced proteomic changes in susceptible cells and protein-lead interaction using Cellular Thermal Shift Assay (CETSA). We integrated above proteome-wide data with bio-databases in an enrichment and network analysis-based inference framework, which helps us identified lead target proteins and signaling pathways involved in the diversified toxicities of lead in different immune cell types. Overall, it forms a lead-immune system interactome upon chronic lead exposure across cellular and molecular levels, which provides unprecedented panoramic information for proactive prevention, therapy formulation and public health evaluation.

Materials and methods

Experimental design

This study was designed to use mass cytometry (CyTOF) to examine single-cell lead distribution and the strength of thiol metal scavenging system in different immune populations from C57BL/6 mice treated with lead nitrate by intragastric administration (i.g.). The RBC and leukocytes were separated from peripheral blood, spleen and lymph node. The absolute amount of lead was determined using inductively coupled plasma mass spectrometry (ICP-MS). Percoll separated splenic immune cells, purified naïve CD4 + T cells and cell lines were used for functional and proteomic study. Experiments were triplicated, and only replicable results were chosen.

Cell culture

HL-60 (ATCC® CCL-240 TM) cells were cultured in a humidified atmosphere of 5% CO_2 at 37 °C with IMDM (Iscove's Modified Dulbecco's Medium, Gibco 12,440–053) containing 12% fetal bovine serum (FBS, Gibco 10,438–026) and 100 U/mL penicillin–streptomycin (Gibco 15,140–122). HL-60 cells were incubated in the above medium containing 1.25% DMSO (v/v) for 6 days to further differentiate into neutrophils (dHL-60). HEK293 T (ATCC® CRL-3216) cells were cultured in a humidified atmosphere of 5% CO_2 at 37 °C with DMEM (Dulbecco's Modified Eagle Medium, Gibco 12,100–046) containing 12% fetal bovine serum (FBS, Gibco 10,438–026) and 100 U/mL penicillin–streptomycin (Gibco 15,140–122).

Animal experiments

C57BL/6 mice (male, 7 weeks old, 15–25 g) were treated (i.g.) either without or with 60 mg lead nitrate and 450 mg Bucillamine per Kg body weight daily for 4 weeks before sampling. The volume of water consumed by each mouse was carefully measured and recorded as the volumes of waters consumed per mouse per day. All mice were anaesthetized with isoflurane before sampling and sacrificed by manual cervical dislocation. Peripheral blood, lymph nodes and spleen were collected for further analysis. All animals had acclimatized for 1 week after arrival. All studies were performed at Shanghai Jiao Tong University in accordance with the Shanghai Jiao Tong University Institutional Animal Care and Use Committee (IACUC) guidelines (Animal ethical permission No: BME-2019043).

Chemicals and reagents

Cisplatin was obtained from Sigma-Aldrich (St. Louis, MO, USA). Metal-labelled antibodies, MAXPAR ® X8 labeling reagent kits and Cell-ID™ IdU were purchased from Fluidigm Corp (South Francisco, CA, USA). Non-metal-labelled and BSA-free antibodies were purchased from Abcam Trading (Shanghai) Company Ltd (Shanghai, PRC) and Biolegend (San Diego, CA, USA). See Table S1 for the panel of antibodies. Lead nitrate (No.80073614) was purchased from SinoPharm Ltd (Shanghai, PRC). L-Buthionine-sulfoximine (L-BSO) was obtained from Sigma-Aldrich (St. Louis, MO, USA). RNAiso Plus for RNA extraction was purchased from TAKARA Bio Inc (Shanghai, PRC).

Percoll separation of immune cells

Percoll density gradient centrifugation was used to separate immune cells from cell samples. Percoll was diluted using PBS. Blood was centrifuged at 400 g for 5 min to separate serum from blood cells. The blood cells were then mixed with Percoll to form a final 40% percoll concentration. Without disturbing the interface, cell-containing 40% percoll was carefully loaded on an 80% percoll layer, and centrifuged at 400 g for 30 min. immune cells were carefully collected from the interface between the 40% and 80% Percoll layer.

Mass cytometry by time of flight (CyTOF)

All cell samples were processed according to standard protocol provided by the manufacturer (Fluidigm Protocol PN 400276). Each sample contained two million cells (in 2 ml water). Cells from each sample were either left untreated or stimulated for 4 h using eBioscience™ Cell Stimulation Cocktail (500X), which contains phorbol-12-myristate-13-acetate (PMA) and ionomycin. 2 μM Cisplatin was added to cells for 5 min as an indicator of dead cells, the staining was terminated by addition of 2 ml of Cell Staining

Buffer (Fluidigm). The cells were centrifuged (500 g for 5 min), the supernatant was removed and incubate with anti-CD16/32 antibody at room temperature for 10 min. The cells were then stained with a mixture of metal-tagged antibodies at room temperature for 30 min (For the complete list of antibodies, please see Supplementary Table. S1). Metal pre-loaded antibodies were validated by the manufacturers for mass cytometry applications, and metal-labeling of antibodies was prepared using the Maxpar X8 Multimetal Labeling Kit (Fluidigm Corp) according to manufacturer's instructions. Optimal concentrations were determined by titration. The cells were then washed twice with Cell Staining Buffer, the supernatant was removed, 100 µl of calcium and magnesium-free PBS was added, and the cells were vortexed for 5 s. The suspended cells were then stained using Cell-ID™ Intercalator-Ir (Fluidigm) according to the manufacturer's guide (available online). The cells were finally washed once using Cell Staining Buffer and three times with deionized water before CyTOF examination. The CyTOF instrument (Fluidigm Corp, South Francisco, CA, United States) was cleaned, tuned and calibrated before experiments. Argon gas was used for generating the plasma and nebulizing cell suspension. Processed samples were applied to CyTOF, with a flow rate of 30 µl/min, measured in a dual instrument mode. The raw data were generated as standard FCS file, randomized and normalized by Software Helios version 6.5.358 (Fluidigm Corp, South San Francisco, CA, United States). Data were analyzed using Python.

Inductively Coupled Plasma Mass Spectrometry (ICP-MS)

ICP-MS was used to monitor the cellular levels of all interested metals. Harvested tissue culture cells were dissolved by 0.2 mL of 50% HNO3 and 50% H_2O_2 (1:1 volume ratio) at 60 °C for 1 h using a Thermolyne Dri-Bath. The dissolved samples were diluted to appropriate concentration for quantification of metals using ICP-MS. Metal quantifications were triplicated and average values were used.

Protein lysis and digestion for proteomics analysis

Medium was aspirated, cells were washed with ice-cold PBS three times. Cells were scraped and collected in 1.5 ml vials. Cells were pelleted by centrifugation for 5 min at 800 × *g* at 4 °C. Cell pellets were snap-frozen in liquid nitrogen and stored overnight at − 80 °C until further analysis. Pellets were thawed, cells were lysed with buffer (Beyotime) containing 50 mM Tris (pH 7.4), 150 mM NaCl, 1% Triton X-100, 1% sodium deoxycholate, 0.1% SDS, supplemented with complete protease inhibitor mixture (Beyotime). Cells were placed on the ice for 30 min, sonicated for 15 cycles of 30 s. The total protein concentration was determined using a BCA assay (Thermo). Then cells were heated for 5 min at 95 °C. Proteins were first desalted with acetone, then reduced with 7 M DTT and alkylated with 1 M IAA respectively. Proteins were digested overnight at 37 °C with trypsin (Promega) with an enzyme to substrate ratio of 1:50. Samples were desalted using Sep-Pak C18 cartridges (Waters), eluted with 60% acetonitrile (ACN)/0.1% formic acid (FA) and directly subjected to peptide enrichment. The total peptide concentration was determined using Pierce™ Quantitative Colorimetric Peptide Assay (Thermo). Samples for proteome analysis were instead dried down and stored at − 80 °C until subjected to nLC-MS analysis.

Reverse phase chromatography and mass spectrometry

Peptides were subjected to reversed phase nLC-MS/MS analysis using an Easy nLC1200 system coupled to a Q Exactive HF-X mass spectrometer (Thermo Fisher Scientific) for the proteome analysis. The chromatograph system was equipped with a trap column (Acclaim PepMap™ 100, 75 µm × 2 cm, C18, 3 µm, 100 Å) and an analytical column (Acclaim PepMap™ RSLC, 75 µm × 25 cm, C18, 2 µm, 100 Å). Trapping was performed for 3 min in solvent A (0.1% FA in water) at 2 µl min^{-1}, while for the elution the flow rate was passively split to 300 nl min^{-1}. The gradient was as follows: 0–1 min, 8% buffer B (0.1% FA in 80% ACN); 1–98 min, 8% to 28% buffer B; 98–112 min, 28% to 36% buffer B; 112–116 min, 36% to 100% buffer B; 116–120 min, 100% buffer B.

The mass spectrometer was operated using Xcalibur (version 4.1, Thermo Scientific) in data-dependent mode. The Orbitrap full-scan MS spectra from m/z 350–1800 were acquired at a resolution of 60,000 after accumulation to a target value of $3e^6$. The maximum ion injection time was 20 ms. Up to twenty most

intense precursor ions were selected for fragmentation, with the isolation window set to 1.6 m/z. HCD fragmentation was performed at normalized collision energy of 28% after the accumulation to a target value of $2e^5$, with the maximum injection time of 25 ms. MS/MS was acquired at a resolution of 15,000. Dynamic exclusion was set to 60 s.

Cellular Thermal Shift Assay (CETSA)

HEK-293 T cells were harvested, washed with PBS and diluted in PBS containing protease inhibitor cocktail. The cell suspensions were freeze-thawed three times using liquid nitrogen and then centrifuged at 20,000 ×g for 20 min at 4 °C. The supernatants were collected and diluted with PBS containing protease inhibitor cocktail and divided into aliquots (50 µL), 5 aliquots being treated with different concentrations of lead nitrate and one aliquot was treated with water as a control. After a 30-min incubation at room temperature the lysates were heated at 52 °C for 3 min and cooled at 25 °C for 3 min (A600 Super Gradient Thermal Cycler, LongGene). The lysates were centrifuged at 20,000 ×g for 20 min at 4 °C. The soluble fractions were separated from precipitates and transferred to new microtubes. The final supernatants were analyzed with the proteomic analysis procedure described above.

Glutathione assay

Collected cell samples were homogenized in assay buffer (100 mM potassium phosphate, pH 7.0, 5 mM EDTA), frozen and thawed twice, and centrifuged at 10, 000 g, 4 °C for 10 min. The supernatant was then used for further experiments. The intracellular glutathione levels were measured colorimetrically based on reduction of 5,5-dithiobis (2-nitrobenzoic acid) (DTNB) into TNB by glutathione. TNB absorption at 405 nm was used for quantification. In the presence of NADPH and glutathione reductase (GR), the oxidized GSH and the original GSSG were both continuously reduced back to GSH and interact with DTNB to produce TNB. The reaction was measured by kinetic reading at 405 nm (1 min interval for 5 min). The slope of absorption at 405 nm through time represents the level of glutathione.

Purification of murine naïve CD4 + T cells

Murine naïve splenic CD4 + T cells from C57BL/6 mice were negatively enriched by MojoSort Mouse CD4 Naïve T cell Isolation Kit (BioLegend). Purified CD4 + naïve T cells were used for ELISA or proteomic study.

Routine blood test

Blood samples were collected from the orbital sinus of mice with anticoagulant tubes (367,878, BD Vacutainer, USA). 100 µl of whole blood samples were injected into routine blood tests via an automatic hematology analyzer.

Flow cytometry

The blood mononuclear cells were purified with Percoll buffer and stained with CD45-FITC (BD Pharmingen, USA, Cat# 553,080), CD3-BV421 (BD Pharmingen, USA, Cat# 562,600), CD4-BV510 (BD Pharmingen, USA, Cat# 563,106), CD8-PE-Cy7 (BD Pharmingen, USA, Cat# 552,877). Flow cytometry was performed using BD FACSA instrument and the data were analyzed using *Flowjo* software.

Manual Gating of CyTOF data

Manual gating of mass cytometry data was performed using Python. A hierarchical gating strategy was used to identify live, single cells of main immune cell subsets based on the expression of protein markers. This gating strategy is derived from the procedure that assay manufacturer has provided (Fluidigm, PRD013-201306 V7, attached in supplement).

Data visualization

The CyTOF data are visualized using algorithms T-distributed Stochastic Neighbor Embedding (*t*-SNE) and Principal Component Analysis (PCA). *t*-SNE visualization was performed using Python TSNE module from sklearn.manifold. Default parameters were used. PCA visualization was performed using Python PCA module from sklearn.decomposition. Default parameters were used. The proteomic data were visualized using Cytoscape, Perfused Force Directed Layout was used.

Databases for proteomic analysis

Multiple databases were used for proteomic data analysis. Gene ontology and annotation databases from http://geneontology.org. Version: Gene Ontology database: format-version: 1.2, data-version: releases/2020–10-09; Gene Ontology Annotation database: gaf-version: 2.1, PANTHER version: v.15.0., GO version: 2020–09–10. String protein interaction database from https://string-db.org. Version 11.0. Protein domain database InterPro from https://www.ebi.ac.uk/interpro/. Release 84.0, 11 th February 2021.

Statistical analysis

Data were analyzed and visualized using Excel, Graphpad Prism, Cytoscape and Python scipy.stats. Results were all presented as mean ± SD. Each measurement was at least triplicated. The statistical significance was examined using the Student's t-test. Statistical significance was $P < 0.05$. Power analysis was performed with Cohen's effect size = 0.8, significance = 0.05, sample sizes required for all experiments were satisfied.

Results

Single-cell landscape of lead in immune cells and the extreme cell types

Mass cytometry (CyTOF) is a single-cell version of inductively coupled plasma mass spectrometry (ICP-MS), which can simultaneously quantify multiple metal isotopes in single-cell manner. Here, we use CyTOF to study lead's distribution among different immune cells. Firstly, we extract immune cells from blood, spleen and lymph nodes of C57BL/6 mice. Then, we labeled the cells with a panel of 33 metal isotope-tagged antibodies against immune cell markers for cell phenotyping (Table S1). Finally, we quantified single-cell levels of the 33 metal isotopes and 208Pb (most abundant lead isotope) using CyTOF.

Single cell lead levels of total immune cells were visualized using T-distributed Stochastic Neighbor Embedding (*t*-SNE) algorithm, major immune cell types were identified by manual gating according to their expression level of phenotypic markers (Fig. S1), and 208Pb signal intensities in each single cell were presented by colors (Fig. 1A). It shows a highly heterogeneous lead distribution among different immune cells. Among all immune cells, neutrophils (Fig. 1A, *arrow head*) and a subset of splenic dendritic cells (DC) (Fig. 1A, *star*) possess the highest levels of lead. RBCs harbors 10 times more lead than general immune cells (Fig. 1B, *arrow*). Among all immune cells, neutrophils has the highest overall level of lead (Fig. 1B, *arrow heads*), but a portion of splenic DCs have the highest level of lead that is comparable to lead level in RBCs (Fig. 1B, *star*).

In general, innate immune cells have higher lead level than lymphocytes (Fig. 1C). Specifically, lead levels are the highest in splenic DCs and neutrophils, and lowest in the lymphocytes. In terms of the origin of immune cells, blood and splenic immune cells have higher lead levels than lymph node immune cells, which could be explained by the fact that lymph node immune cells are more isolated from blood lead.

Since single-cell lead distribution suggests a highly lead-accumulated splenic DC subtype (Fig. 1A, *star*), to further investigate, we further divided splenic DCs into 4 subtypes, namely lymphoid resident conventional (*lr*-cDC), migratory conventional (*mi*-cDC), plasmacytoid (pDC) and CD14 + monocyte derived dendritic cell (*mo*-DC) (Fig. S2). We found that *mo*-DC is the high lead-containing DC subset in spleen (the *stars* in Fig. 1D), which constitutes only ~ 8% of all splenic DCs, but its lead level is ~ 10 times higher than other splenic DC subtypes. *Mo*-DC is also featured by a high level of 140 Ce (Fig. 1E). Co-existence of such an amount of lead and 140 Ce was also detected in RBC (Fig. 1F), suggesting that *mo*-DC obtained lead by directly engulf RBCs (Korolnek and Hamza 2015).

Single-cell landscape of thiol metabolism in immune cells and the extreme cell types

Biological thiols are critical for lead detoxification in cells. Using CyTOF, we quantified the levels of MT and proteins of GSH metabolism in single immune cells from mice's blood, spleen and lymph node. GSH metabolism proteins detected are glutathione reductase (GR), protein S-glutathionylation, glutamate-cysteine ligase regulatory subunit (GCLM) and multidrug resistance-associated protein 1 (MRP1). Single-cell data are visualized using *t*-SNE, showing

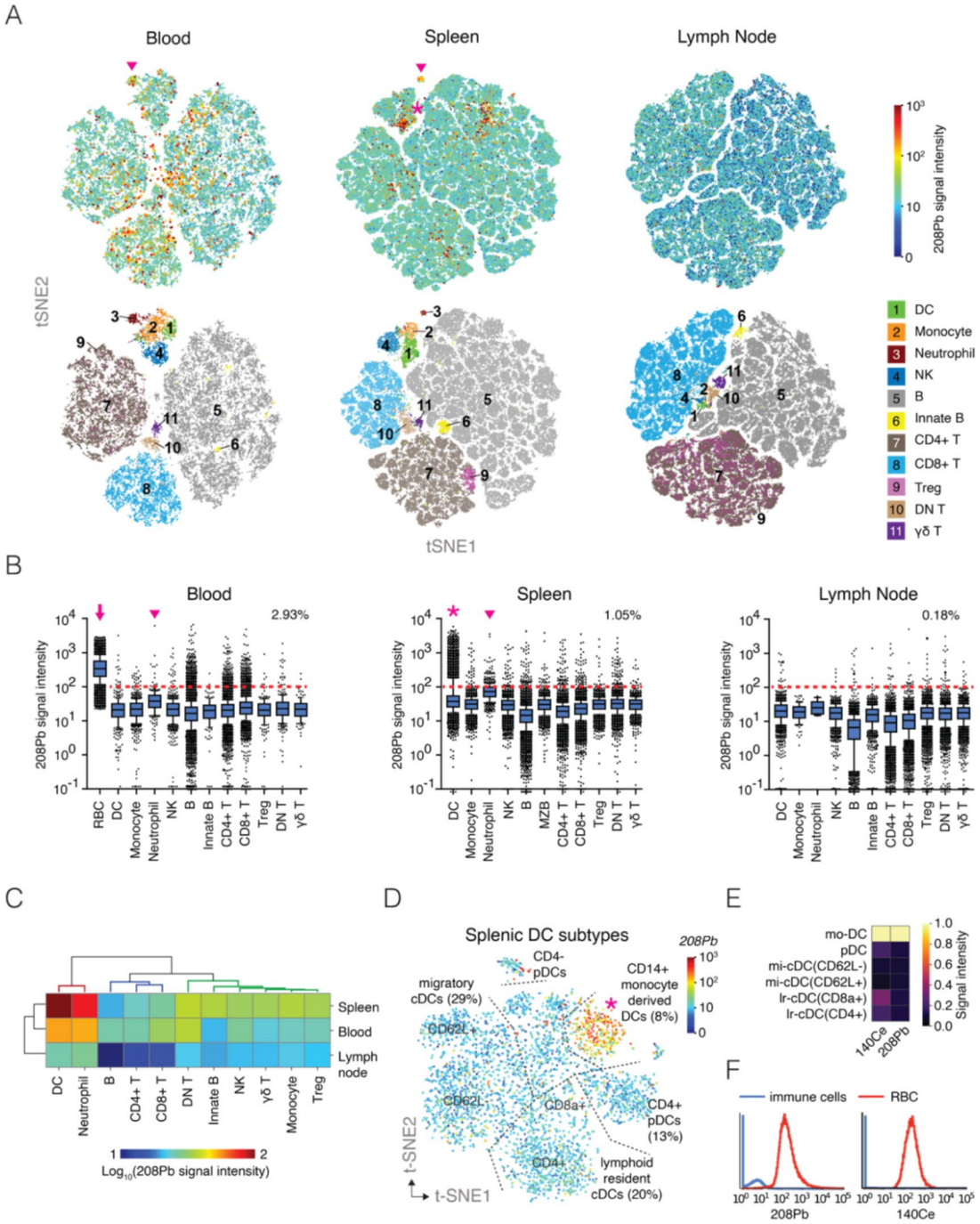

Fig. 1 Single-cell landscape of lead in immune cells and the extreme cell types. (**A**) Single-cell level of lead in immune cells from blood, lymph node and spleen visualized using *t*-SNE. High lead cell clusters are marked with *stars*. (**B**) Clustered heatmap of average lead levels in different immune cell types. (**C**) Single-cell level of lead in splenic DCs visualized using *t*-SNE: lymphoid resident conventional (*lr*-cDC), migratory conventional (*mi*-cDC), plasmacytoid (pDC) and monocyte derived dendritic cell (*mo*-DC). (**D**) Heatmap of average levels of cerium (140 Ce), lead (208Pb) and markers of thiol metabolism in splenic DCs. (**E**) Histogram of single cell 208Pb and 140 Ce level in total immune cells and RBC

a high heterogeneity of thiol metabolism among immune cell types (Fig. 2A). Median expression levels of these proteins in different immune cell types were further analyzed using Principal Component Analysis (PCA), which showed three clusters of cells with distinct features of thiol metabolism (Fig. 2B). In general, immune cells can be divided into three categories: thiol-poor cells, GSH-rich cells, and MT-rich cells. Generally, innate immune cells have higher levels of GSH than lymphocytes, especially neutrophils. Interestingly, the level of GSH conjugate-transporting MRP1 in neutrophils is among the lowest. B cells, especially innate B or marginal zone B cells (MZ B), express highest levels of MT. T cells, especially CD4 + T cells, express lowest levels of both GSH and MT. Overall, CD4 + T cells, neutrophils and MZ B cells

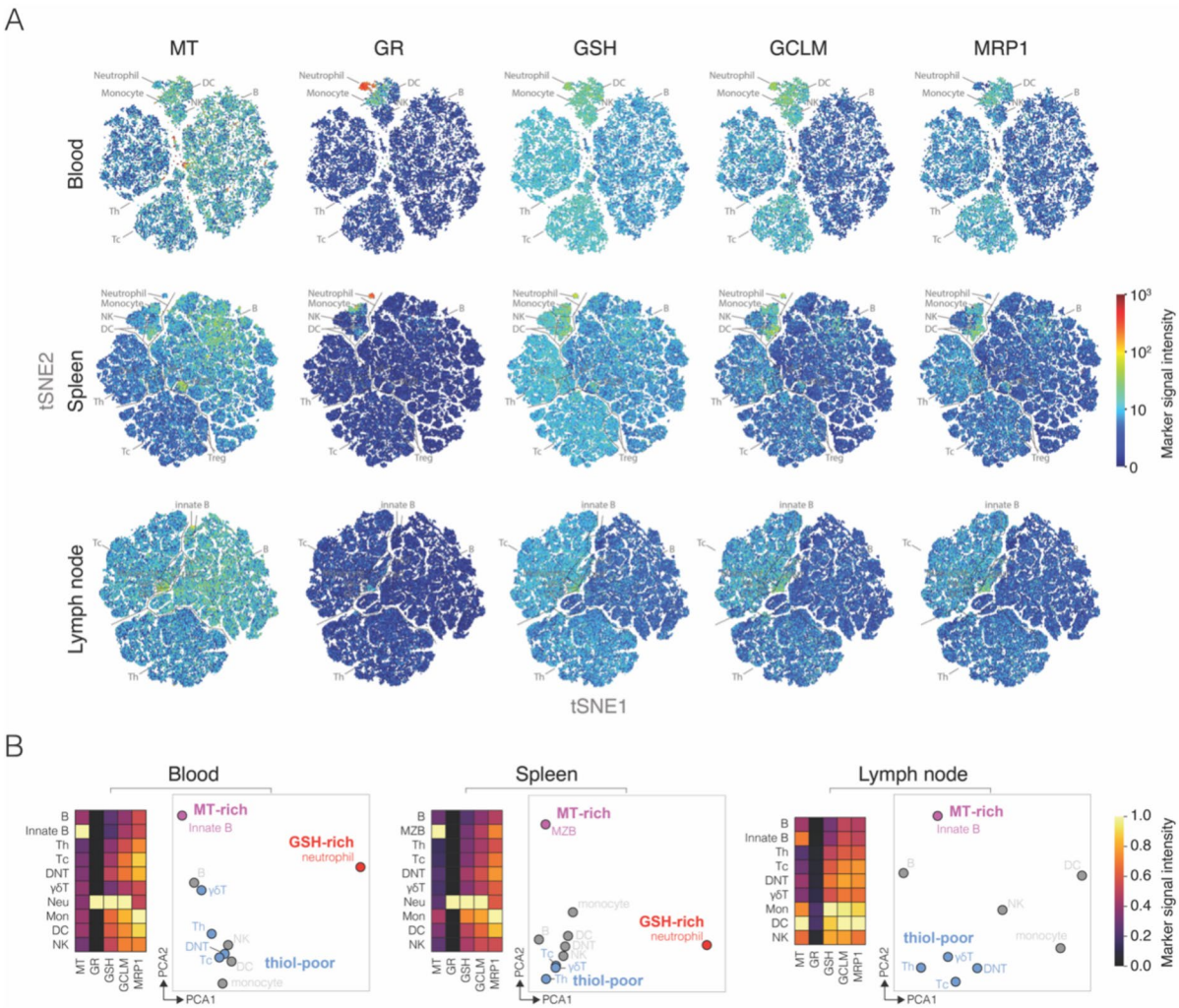

Fig. 2 Single-cell landscape of thiol metabolism in immune cells and the extreme cell types. (**A**) *t*-SNE visualization for single cell levels of metallothionein (MT), glutathione reductase (GR), protein S-glutathionylation (GSH), glutamate-cysteine ligase regulatory subunit (GCLM) and multidrug resistance-associated protein 1 (MRP1) in blood, spleen and lymph node immune cells. Each dot represents a single cell. (**B**) Heatmap showing the median expression level of MT, GR, GSH, GCLM and MRP1 in major immune subsets of blood, spleen and lymph node. All columns in heatmaps are scaled independently to show relative expression of that parameter across cell subsets. On the right of each heatmap are PCA visualization of immune cell subsets according to their median expression levels of MT, GR, GSH, GCLM and MRP1. Neutrophils have the most robust glutathione metabolic capacity (*red*, GSH-rich), innate B and marginal zone B (MZ B) cells have the highest expression levels of MT (*magenta*, MT-rich), and T cells are poor in both GSH and MT (*blue*, thiol-poor)

are respectively the extreme representatives for thiol-poor, GSH-rich and MT-rich category of immune cells. In the next section (Fig. 3), we found that interestingly, thiol-poor CD4 + T cells and GSH-rich neutrophils are also the most vulnerable upon lead exposure, while MT-rich B cells are the most resistant to lead.

Immune cell types with extreme thiol metabolism are most sensitive upon chronic lead exposure

To investigate lead's impacts on immune cells, C57BL/6 mice were treated (i.g.) either without or with 60 mg lead nitrate per kg body weight daily for 4 weeks before sampling (baseline table, Table S2). Lead levels of blood, RBC and serum from lead-treated mice were quantified using ICP-MS, and the values were respectively about 1 μM, 2 μM and 0.1 μM, indicating a mild lead intoxication (Fig. S3). According to WHO report, there are respectively around 815 and 176 million children with blood lead level higher than 5 μg/dl and 10 μg/dl (Rees and Richard 2020). Blood lead level of mice in current study is about 1 μM (20 μg/dl), which indicated a mild lead intoxication close to the case of hundreds of millions of children.

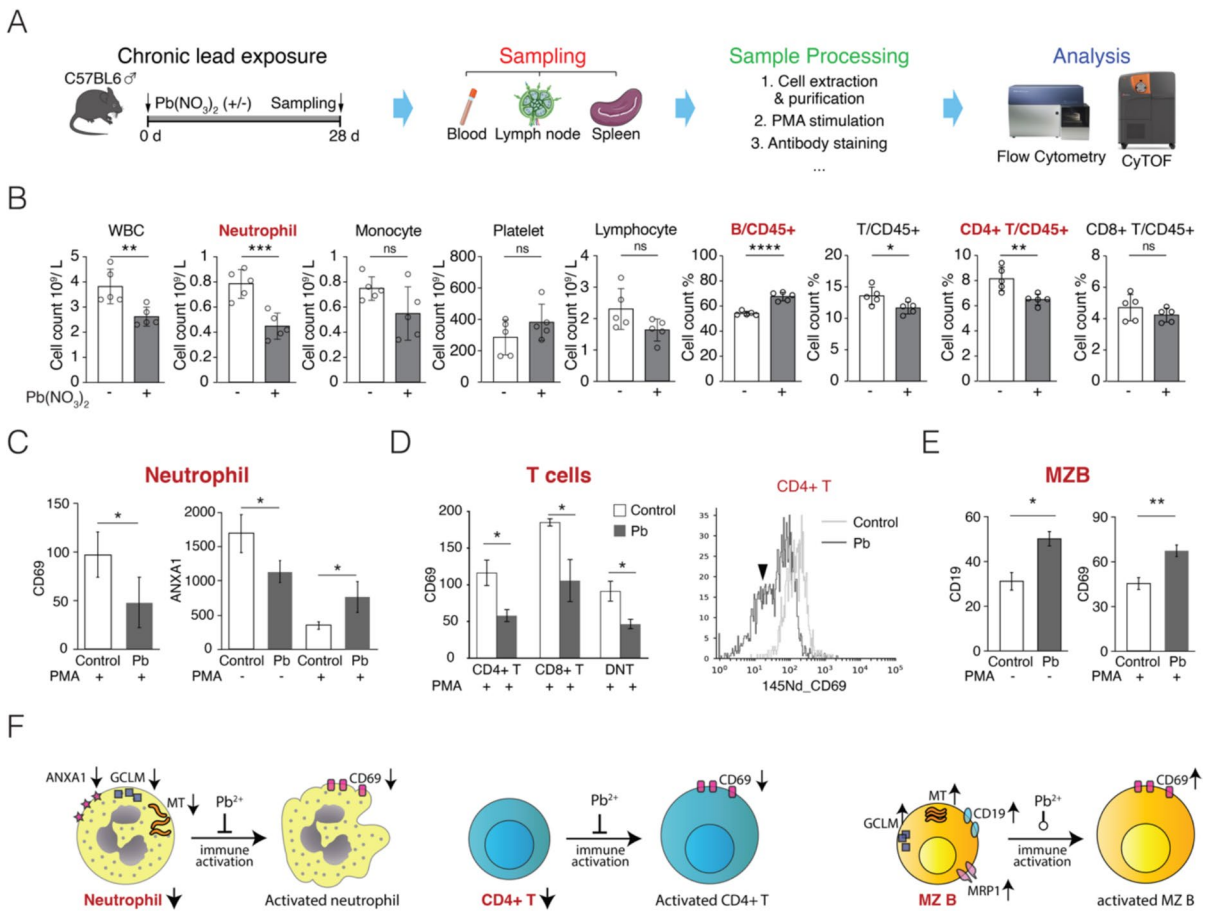

Fig. 3 Immune cell types with extreme thiol metabolism are most sensitive upon chronic lead exposure. (**A**) Experiment procedures of single-cell mass cytometry (CyTOF) in current study. (**B**) Blood immune cell counts in control and lead-treated mice. (**C**) CD69 and ANXA1 levels in neutrophils from control and lead-treated mice without or with PMA/ionomycin stimulation. (**D**) Histogram of CD69 level of PMA/ionomycin stimulated CD4 + T cells from control and lead-treated mice. (**E**) CD19 expression level increase in MZ B cells from lead-treated mice, CD69 expression level increase in PMA/ionomycin stimulated MZ B cells from lead-treated mice. (**F**) Summary of lead's impacts on neutrophils, CD4 + T and MZ B cells. (*P < 0.05; **P < 0.01; ***P < 0.001; ****P < 0.0001; ns, not significant)

Immune cells were extracted from mice blood, spleen and lymph nodes for single-cell study (Fig. 3A). Firstly, we performed a total blood cell count, which showed that the count of white blood cell (WBC), neutrophils, T (especially CD4 + T) cells were greatly reduced, while B cell count was relatively increased in lead-treated mice (Fig. 3B).

To investigate lead's impact on immune functions, we stimulated blood, spleen and lymph node immune cells from control and lead-treated mice with Cell Stimulation Cocktail (PMA/ionomycin) for 4 h before CyTOF examination. As indicated by the expression level of CD69, lead reduced immune activation of neutrophils and T cells, but enhanced the activation of MZ B cells (Fig. 3C-E). Annexin A1 (ANXA1) is involved in neutrophil and T cell function (Perretti and D'Acquisto 2009; Yang et al. 2013; D'Acquisto et al. 2007), which is mainly expressed in neutrophils and other innate immune cells (Fig. S4), and secreted during neutrophil degranulation (D'Acunto et al. 2014). We found that, ANXA1 is 2- fold higher in neutrophils from lead-treated mice after stimulation, suggesting a suppressed degranulation (Fig. 3C). Lead also greatly reduced the activation of T cells, especially the CD4 + T cells (Fig. 3D). MZ B cells express the highest level of MT among all immune cells, which was further increased upon lead exposure (Fig. S5). Lead exposure also increased expression level of B cell antigen receptor (BCR) enhancer CD19 in MZ B cells (Fig. 3E). Interestingly, lead exposure not only did not suppress but also promoted the immune activation of MZ B cells (Fig. 3E). We summarized lead-induced effects in the most sensitive cell types, namely neutrophils, CD4 + T cells and MZ B cells (Fig. 3F).

Proteome-wide survey unveils distinctively different target proteins in lead-sensitive CD4 + T cells and neutrophils

To investigate the mechanism behind lead-induced toxicity in CD4 + T cells and neutrophils, we surveyed lead-induced protein expression changes and protein-small molecule interaction (PSMI) proteome-wide using LC–MS based methods. Firstly, we identified Pb-induced proteomic changes (PIPC) in immune system by performing proteomic analysis on total immune cells, CD4 + T cells and neutrophils (Fig. 4A, Data S1). The samples were splenic immune cells and naïve CD4 + T cells from control and lead-treated mice, and cultured human neutrophils (Fig. S6). Neutrophils were generated by differentiating HL-60 cells with 1.25% DMSO (v/v) for 6 days (dHL-60), and successful modeling was confirmed by increased CD11b expression and triggered NETosis (Fig. S7). We get totally 1306 down-regulated DEPs from all of the above samples (fold of change < = 0.5 and *p*-value < = 0.05). Secondly, we identified Pb-binding proteins by performing Cellular Thermal Shift Assay (CETSA). CETSA is an assay designed to identify PSMI by detecting the thermal stability of proteins without/with ligand binding, with the expectation that ligand binding increases protein thermal stability (Martinez Molina et al. 2013). For CETSA, we incubated HEK293 T cell lysates with 0, 0.01, 0.1, 1, 10, 100 μM lead nitrate in PBS for 30 min before heating and centrifuging. The final product of CETSA was examined by LC–MS proteomics (Data S2). CETSA generates a list of totally 439 Pb-binding proteins (up-regulated DEPs in comparison to control). The number of DEPs peaks at 1 μM of lead, which reflects the fact that lead phosphate solubility in water is 0.67 μM and higher concentration causes precipitation (Fig. S8).

After obtaining above two datasets, we performed both enrichment and Gene Set Enrichment Analysis (GSEA) analysis in perspective of gene ontology molecular function (GOMF) and INTERPRO database (protein domain database) (Fig. 4B). We cross-referenced the outstanding terms between PIPC (down-regulated) and CETSA (up-regulated), and totally identified 113 GOMF or INTERPRO terms outstanding in both experiments. The double outstanding terms contain a total 2065 DEPs or GSEA leading edge proteins (LEPs), cross reference of which with the 1306 down-regulated PIPC DEPs yields 682 DEPs (Data S3). We generated protein–protein interaction (PPI) network of the final 682 double confirmed lead target proteins based on String database, cell type specificities of all DEPs were annotated with colors (Fig. 4C). Among all proteins in PPI network, we identified several clusters of closely related lead target proteins. We found that, ribosomes are the main target of lead in naïve CD4 + T cells, and PKC-like, PE/DAG-binding domain containing proteins and annexins are major targets of lead in neutrophils. Acyl-CoA dehydrogenase, ATP synthase and NADH dehydrogenase in

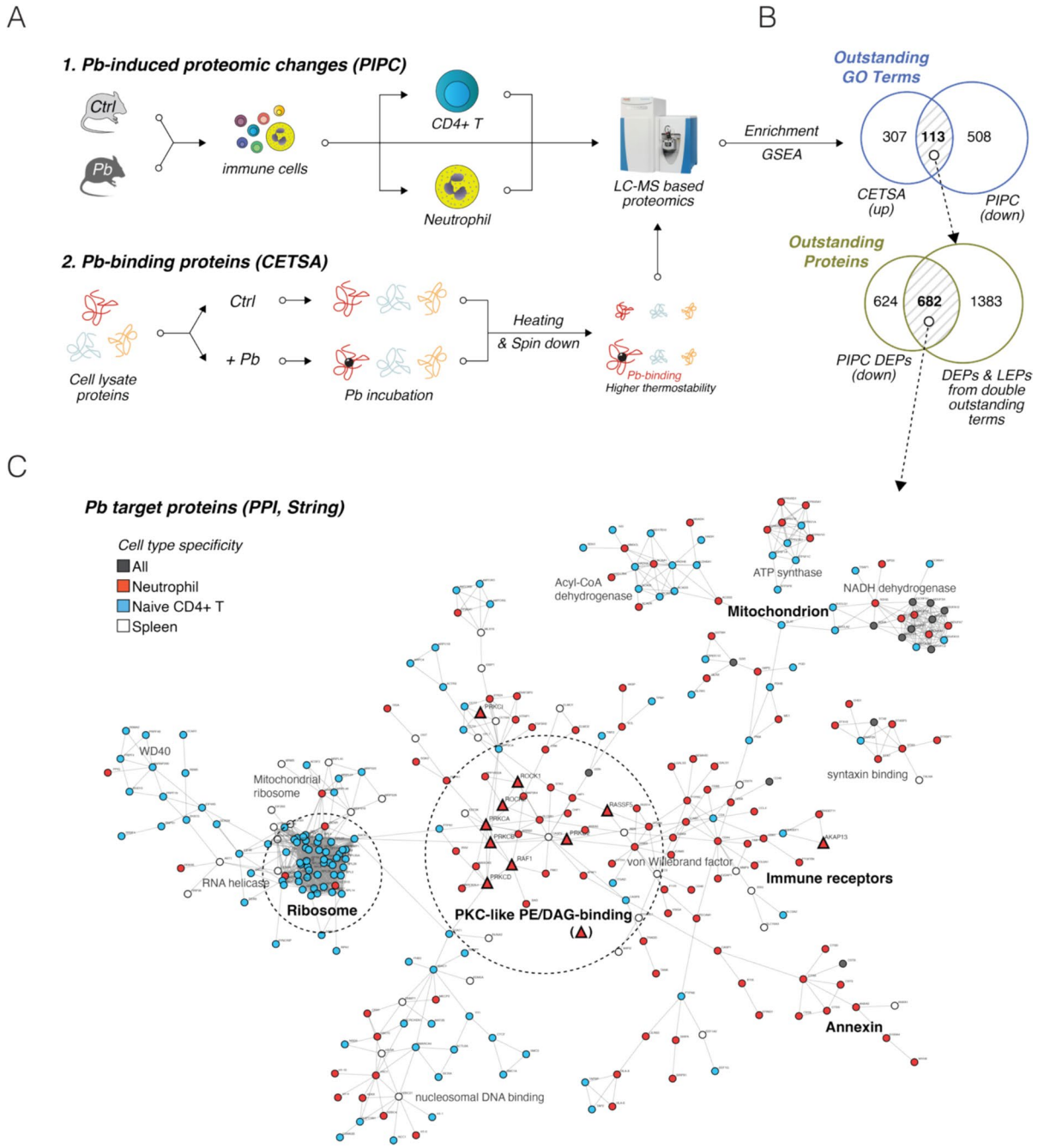

Fig. 4 Proteome-wide survey unveils distinctively different target proteins in lead-sensitive CD4 + T cells and neutrophils. (**A**) Experimental procedures for detection of Pb-induced proteomic changes (PIPC) in CD4 + T cells and neutrophils, and Pb-binding proteins in HEK293 T cell lysate using Cellular Thermal Shift Assay (CETSA). (**B**) Procedure of data analysis of PIPC and CETSA experiment. There are 113 GOMF and INTERPRO terms outstanding in both CETSA (increased thermostability) and PIPC (decreased expression), in either enrichment or GSEA analysis. There are 682 out of 1306 lead-decreased DEPs that belong to CETSA and PIPC double outstanding terms. (**C**) Protein–protein interaction (PPI) network of the 682 DEPs selected in (B). PPI information is based on String database, only interactions with highest confidence (interaction score > 0.9) were selected, proteins not connected to other protein are not shown. Cell type specificity of all DEPs is annotated with colors

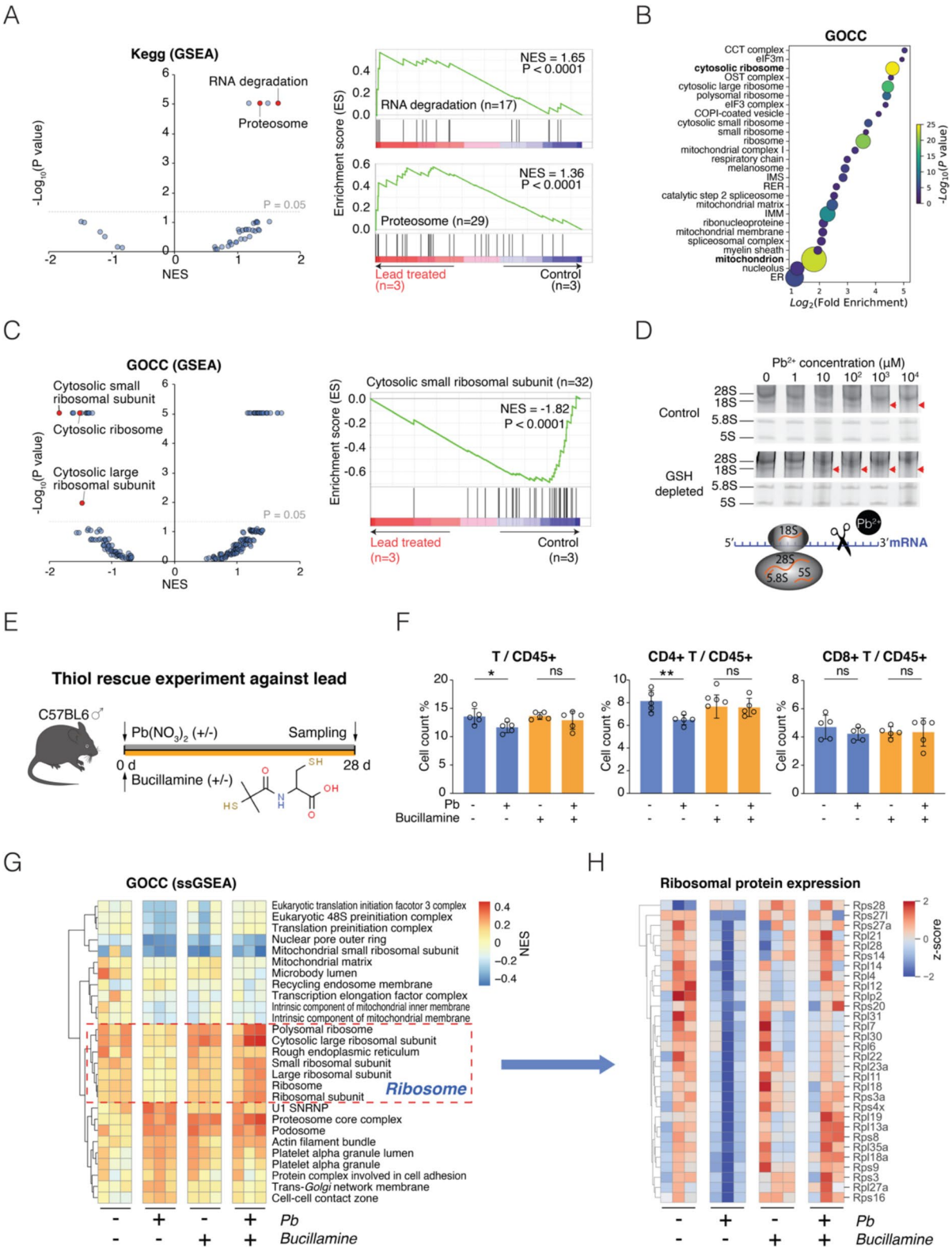
A
Kegg (GSEA)
RNA degradation
Proteosome
P = 0.05
-Log10(P value)
NES
NES = 1.65
P < 0.0001
RNA degradation (n=17)
NES = 1.36
P < 0.0001
Proteosome (n=29)
Enrichment score (ES)
Lead treated (n=3)
Control (n=3)
B
GOCC
CCT complex
eIF3m
cytosolic ribosome
OST complex
cytosolic large ribosome
polysomal ribosome
eIF3 complex
COPI-coated vesicle
cytosolic small ribosome
small ribosome
ribosome
mitochondrial complex I
respiratory chain
melanosome
IMS
RER
catalytic step 2 spliceosome
mitochondrial matrix
IMM
ribonucleoproteine
mitochondrial membrane
spliceosomal complex
myelin sheath
mitochondrion
nucleolus
ER
Log2(Fold Enrichment)
-Log10(P value)
C
GOCC (GSEA)
Cytosolic small ribosomal subunit
Cytosolic ribosome
Cytosolic large ribosomal subunit
P = 0.05
-Log10(P value)
NES
Cytosolic small ribosomal subunit (n=32)
NES = -1.82
P < 0.0001
Enrichment score (ES)
Lead treated (n=3)
Control (n=3)
D
Pb2+ concentration (μM)
0 1 10 10² 10³ 10⁴
Control
GSH depleted
28S
18S
5.8S
5S
Pb2+
5'
3'mRNA
E
Thiol rescue experiment against lead
C57BL6♂
Pb(NO3)2 (+/-)
Sampling
0 d
28 d
Bucillamine (+/-)
F
T / CD45+
CD4+ T / CD45+
CD8+ T / CD45+
*
**
ns
Cell count %
Pb
Bucillamine
G
GOCC (ssGSEA)
Eukaryotic translation initiation facotor 3 complex
Eukaryotic 48S preinitiation complex
Translation preinitiation complex
Nuclear pore outer ring
Mitochondrial small ribosomal subunit
Mitochondrial matrix
Microbody lumen
Recycling endosome membrane
Transcription elongation factor complex
Intrinsic component of mitochondrial inner membrane
Intrinsic component of mitochondrial membrane
Polysomal ribosome
Cytosolic large ribosomal subunit
Rough endoplasmic reticulum
Small ribosomal subunit
Large ribosomal subunit
Ribosome
Ribosomal subunit
Ribosome
U1 SNRNP
Proteosome core complex
Podosome
Actin filament bundle
Platelet alpha granule lumen
Platelet alpha granule
Protein complex involved in cell adhesion
Trans-Golgi network membrane
Cell-cell contact zone
NES
Pb
Bucillamine
H
Ribosomal protein expression
Rps28
Rps27l
Rps27a
Rpl21
Rpl28
Rps14
Rpl14
Rpl4
Rpl12
Rplp2
Rps20
Rpl31
Rpl7
Rpl30
Rpl6
Rpl22
Rpl23a
Rpl11
Rpl18
Rps3a
Rps4x
Rpl19
Rpl13a
Rps8
Rpl35a
Rpl18a
Rps9
Rps3
Rpl27a
Rps16
z-score
Pb
Bucillamine

◂**Fig. 5** Lead-induced CD4 + T cell count and ribosome loss can be rescued by thiol drug. (**A**) GSEA (KEGG) analysis of proteins from naïve CD4 + T cells purified from control and lead-treated mice. It shows that lead specifically induces proteins of RNA degradation and proteasome. (**B**) Enrichment analysis of DEPs in lead-treated splenic naïve CD4 + T cells. Each bubble represents a term, bubble size and color are number of proteins and enrichment *p*-values. (**C**) Volcano plot of GSEA analysis (*left*). Details of cytosolic ribosomal small subunit (*right*). (**D**) Gel electrophoresis of total RNA from control and GSH-depleted HEK293 T cells, treated with lead nitrate for 1 h. Bands of 18S rRNA (*red triangles*). (**E**) Procedures of bucillamine rescue experiment against lead toxicity. (**F**) T, CD4 + T and CD8 + T cell counts in rescue experiment (*P < 0.05; **P < 0.01; ns, not significant). (**G**) Top ssGSEA terms from proteomic data of rescue experiment. (**H**) Heatmap of ribosomal proteins expression in rescue experiment

mitochondrion are lead targets in both naïve CD4 + T cells and neutrophils.

Lead-induced CD4 + T cell count and ribosome loss can be rescued by thiol drug

To unveil the underlying mechanism of lead-induced toxicity in CD4 + T cells, we further scrutinized lead-induced proteomic changes in naïve CD4 + T cells. GSEA analysis against KEGG database indicates that lead greatly increased the expression of proteins for RNA degradation and proteasome, indicating a severe damage to both RNA and protein (Fig. 5A). Enrichment and GSEA analysis in terms of gene ontology cellular component (GOCC) both showed that lead selectively affected ribosomes and mitochondria (Fig. 5B, C).

Thiols are important for lead detoxification, and CD4 + T cells have low thiol levels. Since lead induces ribosome loss mainly in naïve CD4 + T cells (Fig. 5C), to find out whether lack of thiol enabled lead's damage to ribosome, we performed two experiments respectively with GSH depletion and thiol drug supplement.

Firstly, we depleted GSH in HEK293 T cells using L-Buthionine-sulfoximine (L-BSO, inhibitor of glutamate-cysteine ligase (GCL), key enzyme of GSH de novo biosynthesis). Control and GSH-depleted HEK293 T cells were treated with different concentrations of lead for 1 h, then total RNA was extracted for gel electrophoresis (Fig. 5D). Ribosome RNA (rRNA) forms 4 prominent bands sequentially representing 28S, 18S, 5.8S and 5S rRNA, we found that the band of 18S rRNA was significantly reduced and disappeared as lead concentration increased. In GSH-depleted HEK293 T, lead dosage required to diminish 18S rRNA band is lower than that in control cells. 18S rRNA is a component of small ribosomal subunit, which directly binds mRNA. Since exposed mRNAs are highly vulnerable to lead, it could have collaterally affected ribosomes (Palou-Mir et al. 2017).

Secondly, we performed an in vivo rescue experiment with thiol drug (Fig. 5E). Bucillamine is an anti-rheumatic drug that possesses two thiol groups per molecule. C57BL/6 mice were treated (i.g.) either without or with 60 mg lead nitrate and 450 mg Bucillamine per Kg body weight daily for 4 weeks, blood cell count was performed, and total immune cells and naïve CD4 + T cells were purified from spleen of each mouse for proteomic examination. Indeed, bucillamine prevents cell count loss in CD4 + T cells (Fig. 5F), and proteomic data showed that bucillamine rescued lead-induced damage to ribosome (Fig. 5G, H). It indicates that external thiol supplement can effectively rescue lead-induced cell count and ribosome loss in naïve CD4 + T cells. In contrast to naïve CD4 + T cells, bucillamine didn't rescue splenic neutrophils or red pulp macrophages in lead treated mice (Fig. S9), which could be explained by their direct engulfment of highly lead-containing RBCs (Korolnek and Hamza 2015). Overall, we demonstrate thiol is critical in preventing lead-induced damage to RNA and ribosome, which suggests an in vivo lead interacting priority of thiols over RNA.

Robust GSH metabolism selectively damages vesicular metalloproteins in neutrophils upon lead exposure

Among all immune cells, neutrophil has the strongest GSH metabolism (Fig. 2). GSH is known to mediate a detoxification pathway of metals: metal ions enter cells by passive diffusion, which were then first sequestered by GSH and then transported by MRPs into vesicles or out of the cell (Leslie 2012; Mielniczki-Pereira et al. 2008). This process can be quantified using a math model named sequestration-aided passive transport (SAPT) (Fig. 6A) (Hong et al. 2015). To investigate lead metabolism in neutrophils, we treated dHL-60 cells with 5 μM lead nitrate for up to 48 h, cell samples were collected at different time-points for the quantification of lead levels by ICP-MS

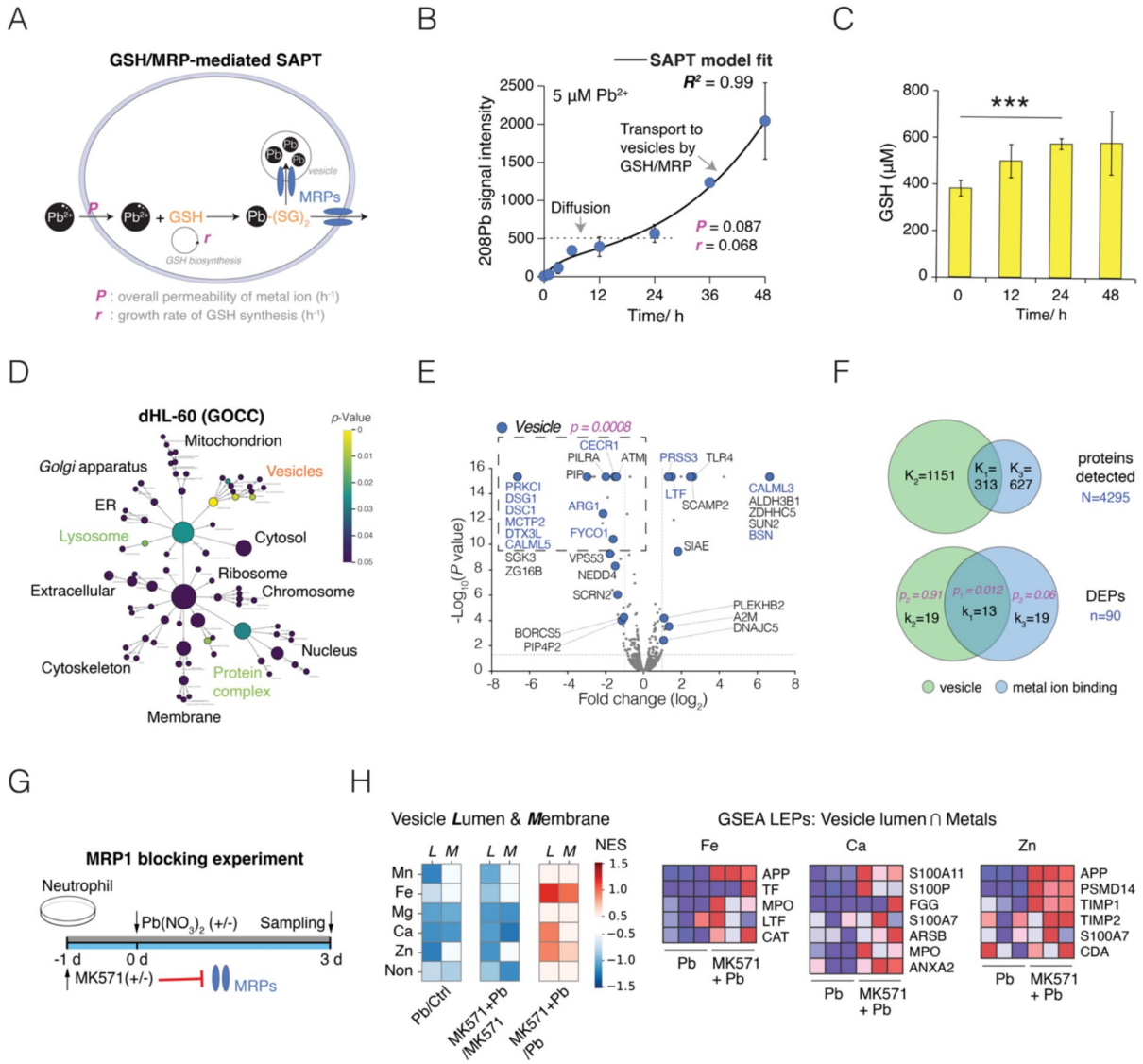

Fig. 6 GSH metabolism selectively damages vesicular metalloproteins in neutrophils upon lead exposure. (**A**) Schematic diagram showing GSH/MRP-mediated sequestration-aided passive transport (SAPT) model, which describes an intracellular disposal mechanism of metal ions by GSH and MRPs. (**B**) Time-dependent lead absorption curve in dHL-60 treated with 5 μM lead nitrate for up to 48 h, fitted with SAPT ($R^2 = 0.99$). (**C**) Total GSH levels in dHL-60 treated with 5 μM lead nitrate for 0, 12, 24 and 48 h (***P < 0.001). (**D**) GO enrichment analysis of DEPs in dHL-60 cells. dHL-60 cells were cultured without or with 1 μM of lead nitrate for 24 h, totally 4295 proteins were identified, 90 of which were DEPs. (**E**) The vesicle DEPs in dHL-60 upon lead treatment, shown as volcano plots. Metalloproteins are blue labeled. (**F**) The Venn plots of vesicle and metal-binding proteins and DEPs in dHL-60 cells. Upon lead treatment, the *p*-values of vesicular non-metal and metal-binding proteins were calculated to be 0.91 and 0.012, respectively. (**G**) Schematic of rescue experiment of lead toxicity to vesicle using MK571 in dHL-60 cells. (**H**) GSEA analysis of dHL-60 cell proteins from rescue experiment in perspective of cross sets between GOCC vesicle lumen/membrane proteins and proteins with different metal ligands. GSEA analysis were performed between Pb and control group, MK571 + Pb and MK571 group, and MK571 + Pb and Pb group. The leading-edge proteins between MK571 + Pb and Pb group of cross sets of vesicle lumen and iron, calcium or zinc-binding proteins were shown on the right

and GSH levels. Indeed, the time-dependent absorption curves of lead by dHL-60 can be well-fitted by SAPT model (Fig. 6B, $R^2 = 0.99$). Saturation of lead in dHL-60 in the first 24 h is characteristic for passive diffusion. The overall permeability P equals 0.087 h^{-1}. Furthermore, GSH was induced 24 h after lead exposure, indicating an activation of GSH biosynthesis (Fig. 6C). The amount of lead in dHL-60 increases exponentially after the activation of GSH biosynthesis, suggesting an enhanced GSH/MRP mediated sequestration of lead into vesicles (Hong et al. 2015).

To investigate lead's impact on neutrophil proteome, dHL-60 cells were treated without or with 5 µM lead nitrate for 48 h, then collected for LC–MS based examinations. Enrichment analysis in perspective of cellular components (GOCC) indicates that lead specifically affects vesicles in dHL-60 cells (Fig. 6D). The expression level of many vesicular proteins, especially the metal-binding proteins, is greatly reduced (Fig. 6E). Further enrichment analysis of cross set of vesicle and metal-binding proteins reveals that, lead selectively affects vesicular metal-binding proteins (p-value = 0.012) instead of vesicular non-metal-binding proteins (p-value = 0.91) (Fig. 6F).

In SAPT model, lead-GSH conjugates are continuously transported into vesicles by MRPs. To validate whether SAPT is behind lead's selective damage of vesicular metalloproteins, we performed LC–MS based proteomic examinations on dHL-60 treated without or with lead and MK571 (MK571 is an MRP inhibitor) (Fig. 6G). Indeed, by GSEA analysis on different metal-binding proteins, we found that lead-induced down-regulation of vesicular metalloproteins can be mitigated by MK571 (Fig. 6H), especially the iron, calcium and zinc-binding proteins. It suggests that the impact of lead on vesicular metalloprotein is mediated by GSH/MRP-mediated SAPT.

PKC-like, PE/DAG-binding proteins are potential targets of immune activation retardation in neutrophils upon lead exposure

Robust GSH metabolism facilitates lead sequestration and lead accumulation in neutrophils. Unfortunately, MRP1 expression in neutrophils is low, which suggests not a timely removal of GSH-lead conjugates (Fig. 2B). GSH-heavy metal conjugate is kinetically labile, without timely removal, metal can be transferred to proteins with higher binding affinity (Banci et al. 2010) (Fig. 7A).

In previous proteomic survey, we identified PKC-like, PE/DAG-binding proteins as main target of lead in neutrophils (Fig. 4C). PKC-like, PE/DAG-binding domain contains two HCCC cysteine-rich zinc-binding sites, suggesting a high binding affinity to lead (Fig. 7B). Indeed, according to our proteomic data, the expression level of PKC-like, PE/DAG-binding domain containing proteins was significantly reduced in a one-sided manner (Fig. 7C). Furthermore, GSEA analysis of CETSA data indicated that thermostability of PKC-like, PE/DAG-binding proteins is significantly increased upon lead exposure, which suggests a direct interaction with lead (Fig. 7D).

To identify target proteins responsible for lead's impact on neutrophil biology, we implemented such a process of analysis: 1. Take protein lists of all KEGG pathways; 2. Generate the PPI network using the STRING database for the protein lists of each pathway; 3. Calculate the PPI network centrality of lead target proteins in each KEGG pathway; 4. Pathways and lead target proteins were clustered based on the centrality of lead target proteins in PPI network of each pathway (Data S3, Fig. 7E).

Summing up network centralities across all pathways for each target protein yielded the 3 most biologically influential proteins: PRKCA, PRKCB and RAF1. We have found that lead retarded immune activation in both neutrophils and T cells (Fig. 3C, D). Interestingly, the 3 most biologically influential proteins are all involved with biological pathways critical for immune activation: T cell receptor (TCR) signaling, neutrophil extracellular trap (NET) formation, MAPK signaling and phosphatidylinositol signaling pathway. And surprisingly, PRKCA, PRKCB and RAF1 all contain a PKC-like, PE/DAG-binding domain.

Since RAF1/PKCs are critical for immune activation through downstream MAPK and phosphatidylinositol signaling (Fig. 7F), for validation we treated dHL-60 without or with lead and MK571 (Fig. 6G). Indeed, lead greatly reduced MAPK and phosphatidylinositol signaling in neutrophils, and MK571 enhanced lead-induced suppression of phosphatidylinositol signaling (Fig. 7G, H). Overall, it suggests that in neutrophils not a timely removal of GSH-lead conjugates could further affect RAF1/PKCs, and PKC-like, PE/DAG-binding proteins are potential

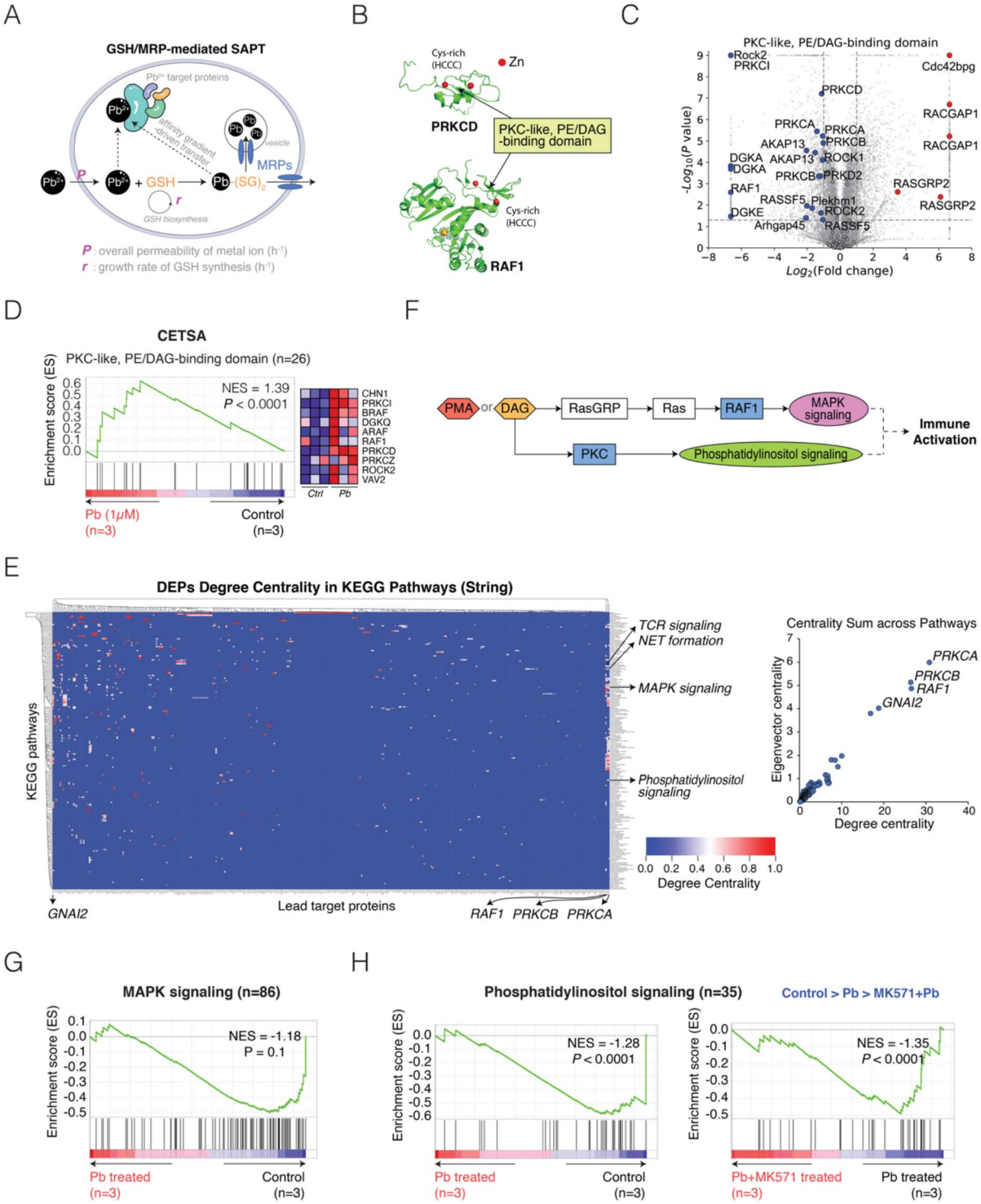
A
GSH/MRP-mediated SAPT
Pb2+ target proteins
affinity gradient driven transfer
vesicle
MRPs
P
GSH
r
GSH biosynthesis
P : overall permeability of metal ion (h-1)
r : growth rate of GSH synthesis (h-1)
B
Cys-rich (HCCC)
Zn
PRKCD
PKC-like, PE/DAG -binding domain
Cys-rich (HCCC)
RAF1
C
PKC-like, PE/DAG-binding domain
Rock2
PRKCI
Cdc42bpg
PRKCD
RACGAP1
PRKCA
PRKCA
PRKCB
AKAP13
RACGAP1
DGKA
AKAP13
ROCK1
DGKA
PRKCB
PRKD2
RASGRP2
RAF1
RASSF5
Plekhm1
RASGRP2
DGKE
ROCK2
Arhgap45
RASSF5
-Log10(P value)
Log2(Fold change)
D
CETSA
PKC-like, PE/DAG-binding domain (n=26)
Enrichment score (ES)
NES = 1.39
P < 0.0001
CHN1
PRKCI
BRAF
DGKQ
ARAF
RAF1
PRKCD
PRKCZ
ROCK2
VAV2
Ctrl
Pb
Pb (1μM) (n=3)
Control (n=3)
F
PMA
or
DAG
RasGRP
Ras
RAF1
MAPK signaling
Immune Activation
PKC
Phosphatidylinositol signaling
E
DEPs Degree Centrality in KEGG Pathways (String)
KEGG pathways
TCR signaling
NET formation
MAPK signaling
Phosphatidylinositol signaling
Centrality Sum across Pathways
PRKCA
PRKCB
RAF1
GNAI2
Eigenvector centrality
Degree centrality
Degree Centrality
GNAI2
Lead target proteins
RAF1 PRKCB PRKCA
G
MAPK signaling (n=86)
Enrichment score (ES)
NES = -1.18
P = 0.1
Pb treated (n=3)
Control (n=3)
H
Phosphatidylinositol signaling (n=35)
Control > Pb > MK571+Pb
Enrichment score (ES)
NES = -1.28
P < 0.0001
Pb treated (n=3)
Control (n=3)
NES = -1.35
P < 0.0001
Pb+MK571 treated (n=3)
Pb treated (n=3)

◂**Fig. 7** PKC-like, PE/DAG-binding proteins are potential targets of immune activation retardation in neutrophils upon lead exposure. (**A**) Schematic diagram showing GSH/MRP-mediated sequestration-aided passive transport (SAPT) model and affinity gradient driven ion transfer. (**B**) Protein structure of the PKC-like, PE/DAG-binding domain from RAF1 (6XBH) and PKCD (2YUU). (**C**) Volcano plot of lead-treatment DEPs of INTERPRO term: PKC-like, PE/DAG-binding domain. (**D**) GSEA results of INTERPRO term: PKC-like, PE/DAG-binding domain showing a significantly increased thermostability upon lead in CETSA experiment. (**E**) DEPs degree centrality in KEGG pathways based on String database (*upper, heatmap*). Protein degree and eigenvector centrality across all KEGG pathways (*right*). (**F**) A subgraph of KEGG pathway (Map04660) of DAG activation in immune cells showing the critical position of RAF1, PKC and their downstream MAPK and phosphatidylinositol signaling. (**G**) GSEA analysis showing significantly reduced MAPK signaling in lead treated dHL-60 cells. (**H**) GSEA analysis showing significantly reduced phosphatidylinositol signaling in lead treated dHL-60 cells, and MK571 further enhanced lead-induced suppression on phosphatidylinositol signaling

targets of immune activation retardation in neutrophils upon lead exposure.

Discussion

Lead has been widely used for thousands of years, despite the 1996 ban on leaded gasoline, environmental lead residues and other pollution sources remain. Currently, human blood lead levels vary between 10–100 ppb by country/region, and around one third of children globally have blood lead levels above the alert line (Cisse 2023). Considering the high prevalence of chronic lead exposure, it has been increasingly recognized that there is no safe threshold for lead exposure, and health hazards of lead could have been greatly underestimated. Immune cells are constantly exposed to blood and are highly sensitive to lead (Fenga et al. 2017; Lorenzo et al. 2006; Zhang et al. 2016; Gao et al. 2007; Engstrom et al. 2015; Bussolaro et al. 2008). Unfortunately, due to immune cell type heterogeneity, even though diverse symptoms of lead-induced immunotoxicity have been reported, the underlying mechanism remains largely unknown.

In this study, for the first time, we used mass cytometry to draw single-cell landscapes of thiol metabolism, lead accumulation and lead's impacts in the heterogeneous immune cells upon chronic lead exposure (Fig. 1–3). It shows that neutrophils, naïve CD4 + T cells and splenic RBC phagocytes are the most susceptible upon chronic lead exposure. Using mass spectrometry, protein-small molecule interaction and statistical inference, we further identified lead target proteins and their corresponding signaling pathways in lead-sensitive immune cells, which unveils diversified molecular mechanisms of toxicity upon chronic lead exposure (Fig. 4–7). Overall, we established a lead-immune system interactome across cellular and molecular levels (Fig. 8), which provides unprecedentedly rich panoramic information for proactive prevention, therapy formulation and public health evaluation.

In this interactome, we found that "thiols" of different form played key roles in the diversified immunotoxicity induced by chronic lead exposure, these thiols could be biological thiols (e.g. GSH) or metalloproteins with metal-binding centers containing multiple cysteine residues (e.g. MT, ALAD, PKCs and RAF1), each plays different roles in lead-induced immunotoxicities. Lead selectively reduced cell count and immune activation of CD4 + T cells and neutrophils, which respectively have the lowest thiol and highest GSH metabolism. High vulnerability of CD4 + T cells and neutrophils to lead concur their occurrence frequency in clinical reports (Fenga et al. 2017; Lorenzo et al. 2006). In contrast, B cells express high levels of MT and showed higher resistance upon chronic lead exposure. Meanwhile, about 90% of blood lead locate within RBCs binding to the cysteine-rich zinc-binding site of ALAD (Mani et al. 2018). RBC-engulfing immune cells are thus vulnerable to chronic lead exposure, which cannot be mitigated by thiol chelators (Fig. 1D-F, Fig. S9). Below we elaborate the cases in different immune cell types.

Firstly, naïve CD4 + T cells are so poor in thiols that they need cysteine supply from DCs before activation (in form of GSH) (Yan et al. 2009; Akkari and Joyce 2016). Without thiol protection, RNA hydrolytic lead severely affects RNA and ribosome (Fig. 5) (Dybkov et al. 2006). Supplementation with thiol drugs greatly mitigated lead toxicity to CD4 + T cells (Fig. 5).

Secondly, neutrophil has the highest GSH metabolism among all immune cells (Fig. 2). Our evidence suggests that lead metabolism in neutrophils follows a GSH/MRP-mediated SAPT model (Fig. 6A-C). Unfortunately, neutrophil MRP1 expression is among the lowest (Fig. 2B), together with robust GSH

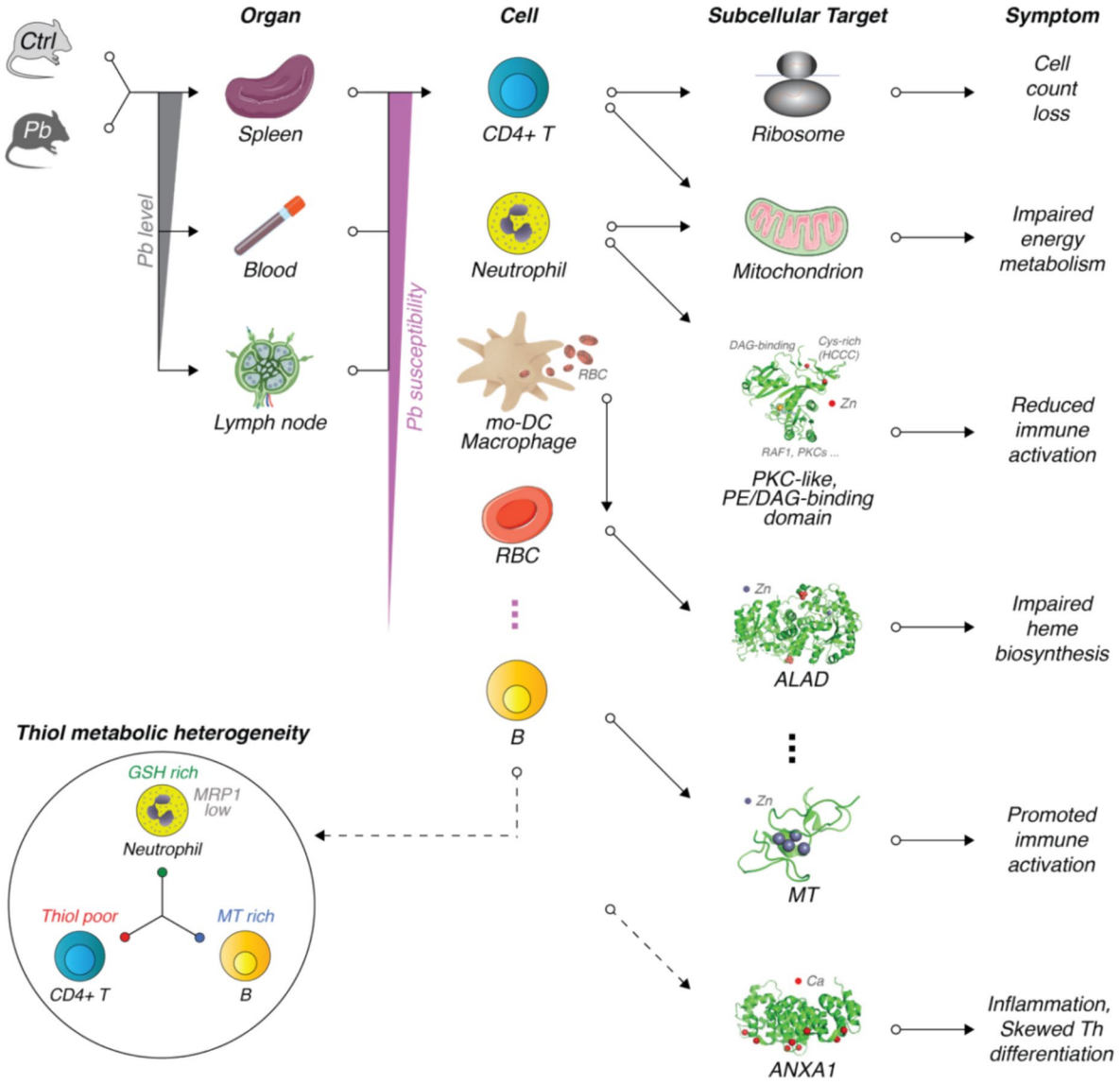

Fig. 8 Multiscale panoramic landscape of lead targets in immune system

metabolism, making neutrophils natural accumulators of lead (Hong et al. 2015; Lim et al. 2020; Jiang et al. 2022). Without timely efflux, Pb^{2+} conjugated to GSH can be passed on to proteins with higher binding affinity (Banci et al. 2010). Our evidence suggests, among these proteins, PKC-like, PE/DAG-binding domain containing protein RAF1 and PKCs are behind lead's suppression of immune activation (Fig. 3C-D, Fig. 7).

PKC has been implicated as a target for Pb^{2+} (Kasten-Jolly and Lawrence 2018). PKC isoforms can be further divided into Ca^{2+}-dependent typical PKC (α, β, γ), Ca^{2+}-independent novel PKC (ε, δ, η, θ) and atypical PKC (μ, ζ, λ). It was found that picomolar (pM) concentrations of Pb^{2+} activate PKC-α but not PKC-ε and PKC-ζ but micromolar (μM) concentrations of Pb^{2+} inhibit all PKCs (Sun et al. 1999). Lead also reduced expression and enzyme activity of all PKC isoforms in neuronal cells (Xu et al. 2006). These results cannot be explained by Pb^{2+} effect on PKC Ca^{2+}-binding site, since some PKC don't have functional Ca^{2+} binding site. In

this study, we found Pb^{2+} significantly reduced the expression of 14 proteins that contain cysteine-rich zinc-binding PKC-like, PE/DAG-binding domain, which includes not only PKCs but also 10 other proteins without Ca^{2+}-binding site, e.g. RAF1, ROCK1, DGKE and AKAP13 (Fig. 7C). It suggests that Pb^{2+} suppresses PKCs by attacking their Zn^{2+}-binding site instead of Ca^{2+}-binding site, further investigation by structural biologists could shed light on this matter.

Thirdly, B cells, especially MZ B cells express high level of MT (Fig. S5). MT's binding affinity to heavy metal is among the top, which might explain B cell's resistance in chronic mild lead exposure (Banci et al. 2010). Lead didn't suppress but instead promoted immune activation in MZ B cells, which could be explained by lead induction of MT and CD19 (Rice et al. 2016; Sugiura and Yamashita 2000; Ishiura et al. 2010) or activation of PKC by low intracellular concentration of lead under MT sequestration (Long et al. 1994) (Fig. 3E).

Finally, the majority of blood lead is bound to ALAD in RBCs on the cysteine-rich zinc-binding site (Mani et al. 2018). Senescent/broken RBCs are recycled by *mo*-DC and macrophage in spleen (Korolnek and Hamza 2015; Klei et al. 2017). *Mo*-DC has the highest lead level among all immune cells, our evidence suggests that it is the result of RBC engulfment (Fig. 1E, F). It was also worth noting that bucillamine could not reduce lead toxicity in red pulp macrophages, suggesting that thiol therapy is not effective for RBC recycling cells (Fig. S6).

Overall, it suggests that lead impairs CD4 + T cells, neutrophils and RBC-phagocytosing immune cells, which in the long run could increase the risk of cancer and infection. In contrast, B cell-based immunity is less affected. Our evidence at cellular and molecular level together suggest that in vivo interaction priority of biomolecules to lead is roughly this: RNA < GSH < lead target metal-binding proteins < MT, and the embodiment of this priority is behind all immunotoxicities induced by chronic lead exposure.

Author contributions Y.H. and X.D. designed research; Y.H., T.Y., H.J., A.W., B.W., Y.L., H.X., C.S. and H.M. performed research; Y.H., T.Y., H.J. analyzed data; T.Y. draw the illustrative figures; Y.H. and X.D. wrote the paper. The authors declare no conflict of interest.

Funding This work was supported by National Key Research and Development Program (2022YFC2601700, 2022YFF0710202), NSFC (T2122002, 22077079, 31900633) and China Postdoctoral Science Foundation GZC20241233.

Data availability All MS data are deposited to ProteomeXchange Consortium via iProX repository with project identifier PXD057344.

Declarations

Competing interests The authors declare no competing interests.

References

Akkari L, Joyce JA. Microenvironmental InterFereNce of metabolism regulates chemosensitivity. Cell Res. 2016;26:867–8.

Banci L, Bertini I, Ciofi-Baffoni S, Kozyreva T, Zovo K, Palumaa P. Affinity gradients drive copper to cellular destinations. Nature. 2010;465:645–8.

Barciszewska MZ, Wyszko E, Bald R, Erdmann VA, Barciszewski J. 5S rRNA is a leadzyme. A molecular basis for lead toxicity. J Biochem. 2003;133(3):309–15.

Bellinger DC. Lead Contamination in Flint–An Abject Failure to Protect Public Health. N Engl J Med. 2016;374:1101–3.

Bussolaro DANIEL, Neto FF, Gargioni ROGÉRIO, Fernandes LC, Randi MAF, Pelletier EMILIEN, Ribeiro CO. The immune response of peritoneal macrophages due to exposure to inorganic lead in the house mouse Mus musculus. Toxicol Vitro. 2008;22(1):254–60.

Cisse N. Saving tens of millions of children a year from the effects of lead poisoning is a surprisingly solvable problem. Nature. 2023;619:674.

D'Acquisto F, Merghani A, Lecona E, Rosignoli G, Raza K, Buckley CD, Flower RJ, Perretti M. Annexin-1 modulates T-cell activation and differentiation. Blood. 2007;109:1095–102.

D'Acunto CW, Gbelcova H, Festa M, Ruml T. The complex understanding of Annexin A1 phosphorylation. Cell Signal. 2014;26:173–8.

Di Lorenzo L, Silvestroni A, Martino MG, Gagliardi T, Corfiati M, Soleo L. Evaluation of peripheral blood neutrophil leucocytes in lead-exposed workers. Int Arch Occup Environ Health. 2006;79:491–8.

Dudev T, Grauffel C, Lim C. How Pb(2+) Binds and Modulates Properties of Ca(2+)-Signaling Proteins. Inorg Chem. 2018;57:14798–809.

Dybkov O, Will CL, Deckert J, Behzadnia N, Hartmuth K, Luhrmann R. U2 snRNA-protein contacts in purified human 17S U2 snRNPs and in spliceosomal A and B complexes. Mol Cell Biol. 2006;26:2803–16.

Engstrom K, Rydbeck F, Kippler M, Wojdacz TK, Arifeen S, Vahter M, Broberg K. Prenatal lead exposure is associated with decreased cord blood DNA methylation of the glycoprotein VI gene involved in platelet activation and thrombus formation. Environ Epigenet. 2015;1:dvv007.

Fenga C, Gangemi S, Di Salvatore V, Falzone L, Libra M. Immunological effects of occupational exposure to lead (Review). Mol Med Rep. 2017;15:3355–60.

Gao D, Mondal TK, Lawrence DA. Lead effects on development and function of bone marrow-derived dendritic cells promote Th2 immune responses. Toxicol Appl Pharmacol. 2007;222:69–79.

Gibbons A. Lead pollution tracks the rise and fall of medieval kings. Science. 2020;368:19–20.

Gibson JM, MacDonald JM, Fisher M, Chen X, Pawlick A, Cook PJ. Early life lead exposure from private well water increases juvenile delinquency risk among US teens. Proc Natl Acad Sci. 2022;119(6):e2110694119.

Hong Y, Lai YT, Chan GC, Sun H. Glutathione and multidrug resistance protein transporter mediate a self-propelled disposal of bismuth in human cells. Proc Natl Acad Sci U S A. 2015;112:3211–6.

Ishiura N, Nakashima H, Watanabe R, Kuwano Y, Adachi T, Takahashi Y, Tsubata T, Okochi H, Tamaki K, Tedder TF, Fujimoto M. Differential phosphorylation of functional tyrosines in CD19 modulates B-lymphocyte activation. Eur J Immunol. 2010;40:1192–204.

Jiang H, Hong Y, Fan G. Bismuth Reduces Cisplatin-Induced Nephrotoxicity Via Enhancing Glutathione Conjugation and Vesicular Transport. Front Pharmacol. 2022;13:887876.

Kasten-Jolly J, Lawrence DA. The cationic (calcium and lead) and enzyme conundrum. J Toxicol Environ Health B Crit Rev. 2018;21:400–13.

Kim HK, Rasnik I, Liu J, Ha T, Lu Y. Dissecting metal ion-dependent folding and catalysis of a single DNAzyme. Nat Chem Biol. 2007;3:763–8.

Klei TR, Meinderts SM, van den Berg TK, van Bruggen R. From the cradle to the grave: the role of macrophages in erythropoiesis and erythrophagocytosis. Front Immunol. 2017;8:73.

Korolnek T, Hamza I. Macrophages and iron trafficking at the birth and death of red cells. Blood. 2015;125:2893–7.

Leslie EM. Arsenic-glutathione conjugate transport by the human multidrug resistance proteins (MRPs/ABCCs). J Inorg Biochem. 2012;108:141–9.

Lim J, Heo J, Ju H, Shin JW, Kim Y, Lee S, Yu HY, Ryu CM, Yun H, Song S, Hong KS, Chung HM, Kim HR, Roe JS, Choi K, Kim IG, Jeong EM, Shin DM. Glutathione dynamics determine the therapeutic efficacy of mesenchymal stem cells for graft-versus-host disease via CREB1-NRF2 pathway. Sci Adv. 2020;6:eaba1334.

Long GJ, Rosen JF, Schanne FA. Lead activation of protein kinase C from rat brain. Determination of free calcium, lead, and zinc by 19F NMR. J Biol Chem. 1994;269(2):834–7.

Makoni M. UN concern over health at site of former Zambian lead mine. Lancet. 2021;398:478.

Mani MS, Kunnathully V, Rao C, Kabekkodu SP, Joshi MB, D'Souza HS. Modifying effects of delta-Aminolevulinate dehydratase polymorphism on blood lead levels and ALAD activity. Toxicol Lett. 2018;295:351–6.

Marshall AT, Betts S, Kan EC, McConnell R, Lanphear BP, Sowell ER. Association of lead-exposure risk and family income with childhood brain outcomes. Nat Med. 2020;26:91–7.

McFarland MJ, Hauer ME, Reuben A. Half of US population exposed to adverse lead levels in early childhood. Proc Natl Acad Sci U S A. 2022;119: e2118631119.

Mielniczki-Pereira AA, Schuch AZ, Bonatto D, Cavalcante CF, Vaitsman DS, Riger CJ, Eleutherio EC, Henriques JA. The role of the yeast ATP-binding cassette Ycf1p in glutathione and cadmium ion homeostasis during respiratory metabolism. Toxicol Lett. 2008;180:21–7.

Molina DM, Jafari R, Ignatushchenko M, Seki T, Larsson EA, Dan C, Nordlund P. Monitoring drug target engagement in cells and tissues using the cellular thermal shift assay. Science. 2013;341(6141):84–7.

Palou-Mir J, Barceló-Oliver M, Sigel RK. The role of lead (II) in nucleic acids. Met Ions Life Sci. 2017;17:403–34.

Pan T, Uhlenbeck OC. A small metalloribozyme with a two-step mechanism. Nature. 1992;358:560–3.

Perretti M, D'Acquisto F. Annexin A1 and glucocorticoids as effectors of the resolution of inflammation. Nat Rev Immunol. 2009;9:62–70.

Rees N, Richard R. The toxic truth: Children's exposure to lead pollution undermines a generation of future potential. A report of UNICEF and pure Earth, New York, NY, USA. 2020;1:90.

Resongles E, Dietze V, Green DC, Harrison RM, Ochoa-Gonzalez R, Tremper AH, Weiss DJ. Strong evidence for the continued contribution of lead deposited during the 20th century to the atmospheric environment in London of today. Proc Natl Acad Sci. 2021;118(26):e2102791118.

Rice JM, Zweifach A, Lynes MA. Metallothionein regulates intracellular zinc signaling during CD4(+) T cell activation. BMC Immunol. 2016;17:13.

Skerfving S, Bergdahl IA. Handbook on the toxicology of metals 4E. In: Nordberg G, Fowler B, Nordberg M, editors. Amsterdam: Academic Press; 2015. vol. 43, pp. 911–956.

Smith TM, Austin C, Green DR, Joannes-Boyau R, Bailey S, Dumitriu D, Fallon S, Grun R, James HF, Moncel MH, Williams IS, Wood R, Arora M. Wintertime stress, nursing, and lead exposure in Neanderthal children. Sci Adv. 2018;4:eaau9483.

Sonne C, Adams DH, Alstrup AKO, Lam SS, Dietz R, Kanstrup N. Denmark passes total ban of leaded ammunition. Science. 2022;377:1054–5.

Sugiura T, Yamashita U. B cell stimulating activity of metallothionein in vitro. Int J Immunopharmacol. 2000;22:113–22.

Sun X, Tian X, Tomsig JL, Suszkiw JB. Analysis of differential effects of Pb2+ on protein kinase C isozymes. Toxicol Appl Pharmacol. 1999;156:40–5.

Xu SZ, Shan CJ, Bullock L, Baker L, Rajanna B. Pb2+ reduces PKCs and NF-kappaB in vitro. Cell Biol Toxicol. 2006;22:189–98.

Yan Z, Garg SK, Kipnis J, Banerjee R. Extracellular redox modulation by regulatory T cells. Nat Chem Biol. 2009;5:721–3.

Yang YH, Morand E, Leech M. Annexin A1: potential for glucocorticoid sparing in RA. Nat Rev Rheumatol. 2013;9:595–603.

Zhang Y, Huo X, Cao J, Yang T, Xu L, Xu X. Elevated lead levels and adverse effects on natural killer cells in children from an electronic waste recycling area. Environ Pollut. 2016;213:143–50.